forests

MDPI

Article

Relationship Between Urban Forest Structure and Seasonal Variation in Vegetation Cover in Jinhua City, China

Hao Yang [1,2,*], Shaowei Chu [1,2], Hao Zeng [1,2] and Youbing Zhao [3]

[1] School of Media Engineering, Communication University of Zhejiang, Hangzhou 310018, China; chu@cuz.edu.cn (S.C.); hao.zeng@cuz.edu.cn (H.Z.)
[2] Zhejiang Key Laboratory of Film and TV Media Technology, Hangzhou 310018, China
[3] School of Computing, University of Derby, Derby DE22 1GB, UK; y.zhao@derby.ac.uk
* Correspondence: yanghao@cuz.edu.cn

Abstract

Urban forests play a crucial role in enhancing vegetation cover and bolstering the ecological functions of cities by expanding green space, improving ecological connectivity, and reducing landscape fragmentation. This study examines these dynamics in Jinhua City, China, utilizing Landsat 8 satellite imagery for all four seasons of 2023, accessed through the Google Earth Engine (GEE) platform. Fractional vegetation cover (FVC) was calculated using the pixel binary model, followed by the classification of FVC levels. To understand the influence of landscape structure, nine representative landscape metrics were selected to construct a landscape index system. Pearson correlation analysis was employed to explore the relationships between these indices and seasonal FVC variations. Furthermore, the contribution of each index to seasonal FVC was quantified using a random forest (RF) regression model. The results indicate that (1) Jinhua exhibits the highest average FVC during the summer, reaching 0.67, while the lowest value is observed in winter, at 0.49. The proportion of areas with very high coverage peaks in summer, accounting for 50.6% of the total area; (2) all landscape metrics exhibited significant correlations with seasonal FVC. Among them, the class area (CA), percentage of landscape (PLAND), largest patch index (LPI), and patch cohesion index (COHESION) showed strong positive correlations with FVC, whereas the total edge length (TE), landscape shape index (LSI), patch density (PD), edge density (ED), and area-weighted mean shape index (AWMSI) were negatively correlated with FVC; (3) RF regression analysis revealed that CA and PLAND contributed most substantially to FVC, followed by COHESION and LPI, while PD, AWMSI, LSI, TE, and ED demonstrated relatively lower contributions. These findings provide valuable insights for optimizing urban forest landscape design and enhancing urban vegetation cover, underscoring that increasing large, interconnected forest patches represents an effective strategy for improving FVC in urban environments.

Keywords: forest landscape; land use; random forest; fractional vegetation cover; Pearson analysis

Academic Editors: Panteleimon Xofis and Craig Nitschke

Received: 26 May 2025
Revised: 4 July 2025
Accepted: 8 July 2025
Published: 9 July 2025

Citation: Yang, H.; Chu, S.; Zeng, H.; Zhao, Y. Relationship Between Urban Forest Structure and Seasonal Variation in Vegetation Cover in Jinhua City, China. *Forests* **2025**, *16*, 1129. https://doi.org/10.3390/f16071129

1. Introduction

Urban vegetation cover encompasses all types of plant communities distributed across urban areas, including trees, shrubs, and grasslands [1]. It plays a crucial role in enhancing urban ecological environments by mitigating the urban heat island effect, reducing air pollution, and improving residents' quality of life [2,3]. By delivering ecosystem services such as

carbon sequestration and oxygen production, urban vegetation significantly contributes to improved air quality [4]. Research indicates that the composition and spatial distribution of vegetation profoundly influence urban ecosystem functions [5]. Different vegetation types offer varying ecosystem services, underscoring the necessity for scientifically informed vegetation structure planning to maximize ecological benefits [6]. Although urbanization often leads to a reduction in green spaces, ecologically driven planning and development strategies can counteract this trend. Initiatives such as the development of urban parks, greenway networks, vertical greening, and rooftop gardens have effectively expanded urban green infrastructure, thereby enhancing both environmental quality and residents' well-being [7].

The urban forest landscape pattern describes the spatial distribution and organization of trees and vegetation within urban areas. Its structure and characteristics are shaped by multiple factors, including land use changes, population density, socioeconomic conditions, and historical context [8,9]. Studies reveal that urban forest composition and structure evolve with land use transitions, such as shifts from natural forests to plantations, which not only diminish biodiversity but also alter ecosystem service functions [10].

In recent years, the influence of urban forest landscape patterns on fractional vegetation cover (FVC) has emerged as a critical research focus [11,12]. FVC refers to the proportion of land surface covered by green vegetation, typically expressed as a continuous value ranging from 0 to 1. This metric effectively captures both the spatial density and the growth status of vegetation. The term "fractional" highlights the proportional nature of the coverage, rendering FVC a quantifiable and continuous ecological parameter widely applied in remote sensing analyses. Urbanization-driven changes in forest landscape patterns affect the distribution and ecological impact of vegetation [13]. Empirical studies have revealed that an increased urbanization intensity is often associated with marked alterations in forest landscape morphology, characterized by rising values of the mean edge area ratio, nearest neighbor distance, and landscape separation index, alongside notable declines in the landscape type area ratio, maximum aggregation index, and patch number index [14]. The mean edge area ratio is used to evaluate the morphological complexity of green space patches; higher values indicate more irregular patch boundaries and a stronger ecological edge effect. The nearest neighbor distance reflects spatial proximity among patches, with lower values indicating more clustered distributions that facilitate species movement and enhance ecological connectivity. Quantitative indicators of green space—such as vegetation coverage, patch count, and total area—are crucial for assessing the scale and spatial distribution of urban vegetation resources. Landscape pattern metrics are instrumental in urban ecological research, as they elucidate the structural influences of green space on ecological processes and provide a scientific foundation for optimizing urban green infrastructure and promoting sustainable urban development. A study of Longquan Mountain Urban Forest Park in Chengdu indicated that FVC first declined and subsequently rebounded between 2014 and 2021, with recovery closely linked to government conservation measures [15]. Similarly, an analysis of landscape patterns in Nanchang's main urban area demonstrated that urban land expansion negatively affected forest vegetation cover, highlighting the ecological challenges posed by urbanization [16].

Landsat 8 satellite imagery, with its high spatial resolution and multi-temporal observational capabilities, has been extensively employed for monitoring and analyzing the dynamics of urban forest vegetation cover [17]. Research has demonstrated that its onboard Operational Land Imager (OLI) sensor captures high-precision data across the visible, near-infrared, and short-wave infrared spectral bands, providing robust support for the extraction of vegetation indices—such as the Normalized Difference Vegetation Index (NDVI)—and for conducting spatiotemporal assessments of urban vegetation change [18].

Numerous empirical studies, including those conducted in Hefei, China, and Chattanooga, Tennessee, USA, have documented a declining trend in forest cover associated with urban expansion. These studies further confirm the high classification accuracy of Landsat 8 imagery and its effectiveness in supporting land cover mapping and the development of related ecological models [19].

Jinhua City, a major regional hub in Zhejiang Province, occupies a strategic location at the crossroads of east–west and north–south transportation networks [20]. However, rapid urbanization and the resulting expansion of urban land have significantly impacted vegetation cover, leading to pronounced changes in the spatial distribution and structure of urban forests [21]. This transformation not only undermines regional biodiversity but also diminishes the ecosystem services provided by forested areas. The consequent reduction in vegetation cover exacerbates the urban heat island effect, threatening urban residents' quality of life and regional ecological stability. Therefore, evaluating the change trajectories of urban forests in Jinhua City is vital for scientific green space planning, enhancing ecological resilience, and addressing urbanization-induced environmental challenges. Optimizing the forest landscape morphology index system can alleviate ecological pressures, improve urban environmental quality, and promote sustainable regional development.

Using Jinhua City as the study area, this research integrates multi-source remote sensing data with landscape ecology theory to systematically investigate the morphological influence of forest landscape patterns on seasonal variations in urban vegetation cover. The primary objective is to elucidate how the spatial structural characteristics of forest patches affect the spatiotemporal distribution of vegetation cover across different seasons. By quantifying the relationships between landscape metrics and FVC, and assessing the seasonal influence of each morphological index, the study provides a theoretical foundation and practical guidance for the optimized configuration of forest landscapes and the enhancement of urban ecological functions.

2. Materials and Methods

2.1. Materials

2.1.1. Study Area

Jinhua City, situated in the central region of Zhejiang Province, spans geographic coordinates from 119°14′ to 120°46′30″ E longitude and 28°32′ to 29°41′ N latitude. Its administrative divisions include Wucheng District, Jindong District, Wuyi County, Pujiang County, Pan'an County, Lanxi City, Yiwu City, Dongyang City, and Yongkang City (Figure 1). The city is endowed with abundant forest resources and a strong ecological foundation, characterized by high forest coverage and a wide distribution of both natural and planted forests, resulting in a diverse and complex forest landscape. Notable forested areas, such as the Shuanglong Scenic Area, Xianyuan Lake Forest Park, and the surrounding mountainous and hilly regions, offer unique ecological advantages. These areas not only contribute significantly to environmental protection and sustainable development but also provide a valuable empirical basis for research on forest landscape patterns and their ecological functions.

Jinhua is located within the central subtropical monsoon climate zone, experiencing four distinct seasons. Spring is marked by a rapid yet variable rise in temperature, with precipitation concentrated in late spring and early summer, often accompanied by hail and strong winds. Summers are hot and prolonged, with high temperatures and frequent rainfall, occasionally interrupted by droughts. Autumn is brief, cool, and humid, while winters are cold, dry, and relatively stable in terms of weather conditions.

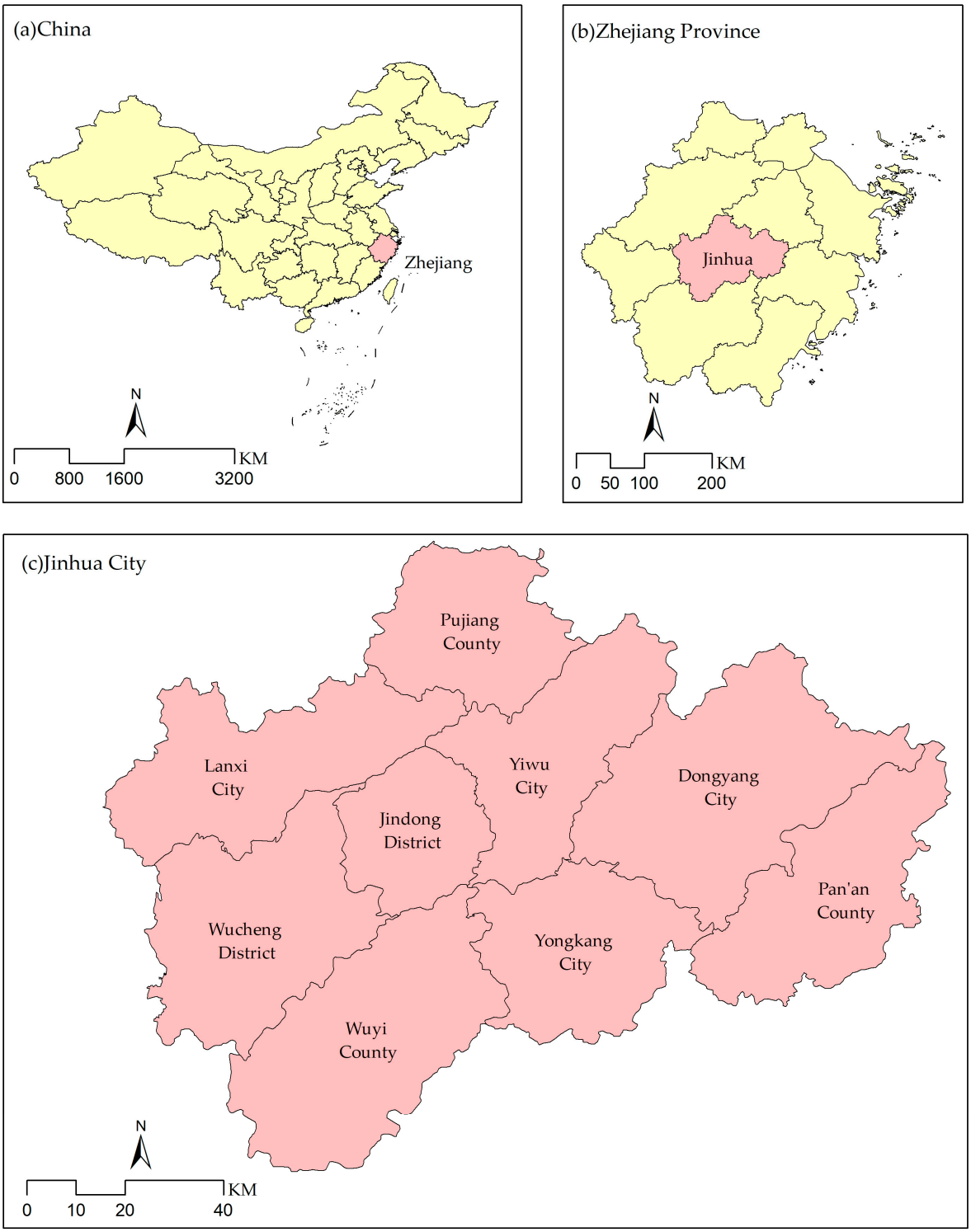

Figure 1. Map of the study area location and scope.

As a key innovation and intellectual hub within the Yangtze River Delta region, and a nationally significant transportation nexus, Jinhua has undergone rapid urban and economic development in recent years. From 2013 to 2023, the impervious surface area increased from 920.14 km^2 to 1107.51 km^2, while the gross regional product more than doubled—from CNY 295.878 billion to CNY 601.127 billion [22,23]. However, this rapid urbanization has exerted considerable pressure on forest resources, leading to spatial compression and ecological degradation. The expansion of impervious surfaces and the concurrent decline in forested areas have significantly impacted urban vegetation cover.

Therefore, a comprehensive investigation into the influence of forest landscape patterns on seasonal variations in urban vegetation cover in Jinhua holds both scientific importance and practical relevance for optimizing urban green infrastructure and enhancing ecosystem service functions.

2.1.2. Data Sources

Google Earth Engine (GEE) is a cloud-based geospatial analysis platform (https://earthengine.google.com/, accessed on 10 April 2025) developed by Google Inc., Mountain View, CA, USA for processing and analyzing remote sensing data. It integrates a vast array of open-access geospatial datasets, including multi-source satellite and aerial imagery, meteorological observations, land surface temperature products, land cover classifications, nighttime light remote sensing data, digital elevation models (DEMs), and various socioeconomic statistical data [24].

In this study, the spatiotemporal dynamics of FVC in Jinhua City across different seasons were systematically analyzed using Landsat 8 satellite imagery from 2023. Landsat 8 provides both Thermal Infrared Sensor (TIRS) data, capable of thermal infrared (TIR) observation, and multispectral data from the OLI, enabling the comprehensive monitoring of vegetation conditions. Landsat 8 was selected as the primary remote sensing data source due to its demonstrated accuracy and widespread application in vegetation cover estimation. The analysis was conducted on the GEE platform, which integrates atmospherically corrected Landsat 8 surface reflectance (SR) products. This correction effectively minimizes the influence of atmospheric interference on surface reflectance, thereby enhancing the reliability of vegetation indices. To ensure the robustness and comparability of vegetation cover estimates across seasons, all images were manually screened for cloud cover and quality anomalies. Leveraging high-resolution remote sensing technology, this study effectively revealed the seasonal and spatial distribution patterns of FVC, providing robust data support for sustainable urban development and ecological management.

Land use data were obtained from the China Land Cover Dataset (CLCD, https://zenodo.org/records/8176941, accessed on 10 April 2025) [25]. This dataset, developed by a research team from Wuhan University, is based on 335,709 Landsat images processed within the GEE platform and provides annual land cover information across China. The team utilized all available Landsat data from GEE to extract spatiotemporal features and employed a random forest classifier for land cover classification. To enhance spatiotemporal consistency, they introduced a postprocessing method combining spatiotemporal filtering and logical inference. According to validation based on 5463 visually interpreted samples, the forest category in this dataset achieves a producer accuracy of 89% and a user accuracy of 86%. The primary advantage of the CLCD lies in its 30 m resolution annual land use classifications, making it highly suitable for fine-scale land cover studies. In this study, the CLCD dataset was used to extract land use information for Jinhua City in 2023, which served as the basis for calculating the forest landscape morphology index.

2.2. Methods

The technical framework of this study (Figure 2) comprises the following key steps: (1) estimation of FVC utilizing the Google Earth Engine (GEE) platform and classification of FVC levels to elucidate its spatial characteristics across different regions; (2) calculation of landscape metrics to quantify landscape pattern characteristics; (3) application of Pearson correlation analysis to evaluate the relationships between seasonal FVC and landscape metrics; and (4) construction of a random forest (RF) regression model to quantify the contribution rate of individual landscape metrics to seasonal FVC.

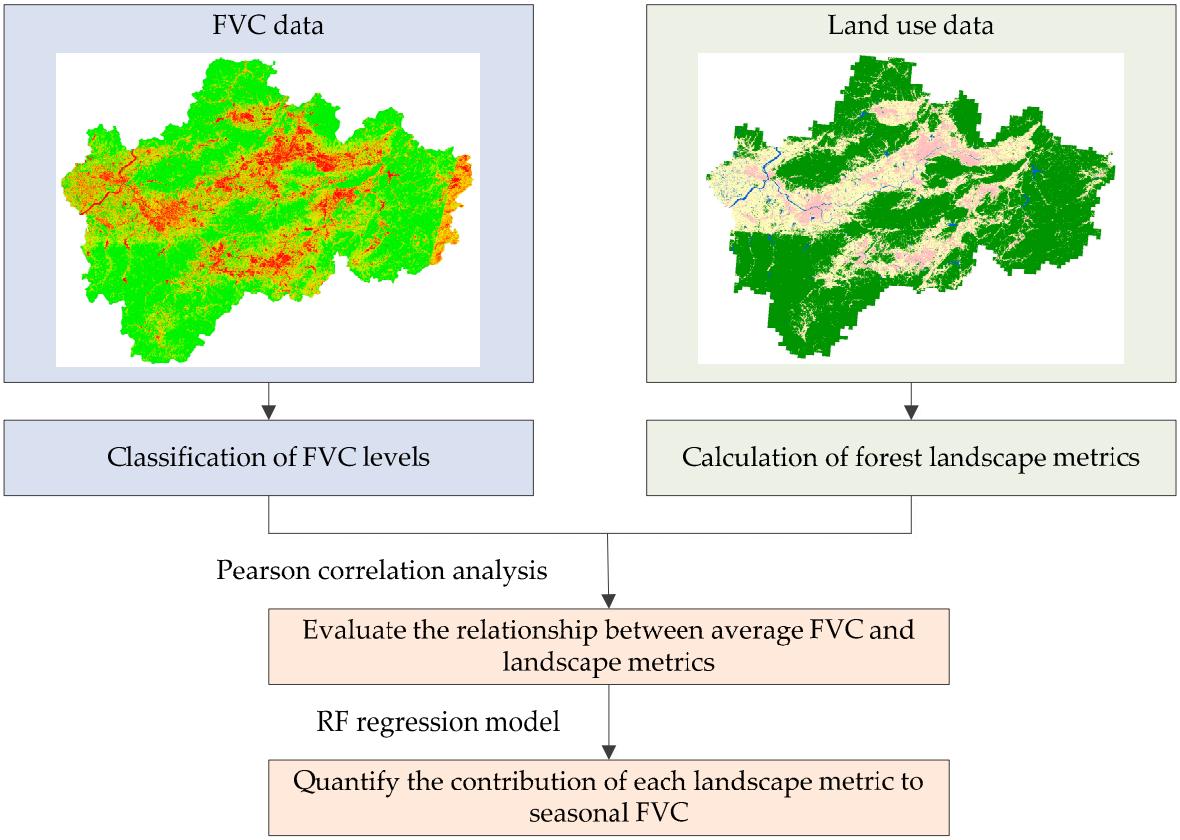

Figure 2. Research methodology roadmap.

2.2.1. Classification of FVC Levels

The GEE platform was employed to calculate the FVC, aiming to enhance data processing efficiency and streamline the traditionally labor-intensive preprocessing workflow. In contrast, conventional methods using ENVI 5.3 software require the manual downloading and correction of remote sensing imagery, alongside reliance on local computational resources, which significantly hinders the efficient processing of large-scale datasets. GEE, leveraging a cloud-computing architecture, enables real-time online processing of extensive multi-temporal remote sensing data while providing abundant free data resources. This cloud-based infrastructure eliminates the need for manual downloading and preprocessing, substantially improving the convenience and efficiency of data analysis [26].

In this study, Landsat 8 remote sensing imagery of Jinhua City for the year 2023 was acquired via the GEE platform to calculate FVC. Landsat 8 offers several notable advantages over Sentinel-2 for calculating seasonal FVC. First, with a continuous data record since its launch in 2013, Landsat 8 provides a longer temporal span and more stable time series, making it particularly suitable for monitoring long-term and seasonal vegetation dynamics [27]. Second, the imagery is distributed by NASA and the USGS with standardized preprocessing workflows and high radiometric calibration accuracy, which enhances the precision and consistency of FVC estimations [28]. Moreover, the global coverage and ease of access to Landsat 8 data facilitate the acquisition of adequate, high-quality imagery across all seasons within the study area.

For the purposes of this analysis, the year 2023 was segmented into four climatological seasons: spring (March–May), summer (June–August), autumn (September–November), and winter (January–February and December). A total of four spring, five summer, four autumn, and three winter Landsat 8 scenes were utilized. Seasonal composite images were generated by applying median synthesis to the image collections for each season

using the GEE platform, thereby producing representative imagery for seasonal vegetation cover assessment.

The NDVI, a widely adopted remote sensing index for assessing vegetation health and coverage, was used as the primary indicator due to its strong linear correlation with vegetation cover [29,30]. The NDVI is computed using the following equation:

$$\mathrm{NDVI} = \frac{\mathrm{NIR} - \mathrm{R}}{\mathrm{NIR} + \mathrm{R}} \quad (1)$$

where NIR represents the near-infrared band value and R denotes the red band value of the Landsat 8 imagery.

To estimate vegetation cover, the pixel-based dimidiate pixel model—a linear unmixing approach—was applied. This model operates under the assumption that each pixel comprises a mixture of vegetated and bare-soil components, influencing the spectral reflectance detected by the remote sensing sensor [31]. Within this model, NDVI values for bare soil ($\mathrm{NDVI_{soil}}$) and fully vegetated areas ($\mathrm{NDVI_{veg}}$) are determined based on the 5th and 95th percentiles of cumulative frequency, respectively [32,33]. The FVC is then calculated using the following formula:

$$\mathrm{FVC} = \frac{\mathrm{NDVI} - \mathrm{NDVI_{soil}}}{\mathrm{NDVI_{veg}} - \mathrm{NDVI_{soil}}} \quad (2)$$

Based on the actual vegetation distribution in Jinhua City, the FVC values were classified into five distinct levels (Table 1).

Table 1. Classification and interpretation of FVC levels.

FVC	Level
FVC < 30%	Very Low Coverage
30% ≤ FVC < 45%	Low Coverage
45% ≤ FVC < 60%	Moderate Coverage
60% ≤ FVC < 75%	High Coverage
75% ≤ FVC	Very High Coverage

2.2.2. Calculation of Landscape Metrics

In this study, the land use types in Jinhua City for the year 2023 were classified into four categories: cropland, forest, water, and impervious surface. The respective areas for each category were 2965.67 $\mathrm{km^2}$ for cropland, 7315.83 $\mathrm{km^2}$ for forest, 151.73 $\mathrm{km^2}$ for water, and 1107.51 $\mathrm{km^2}$ for impervious surface. In this study, the selection of landscape metrics was guided by criteria of representativeness, ecological significance, and data reliability. A total of nine forest landscape indices were selected, including class area (CA), total edge (TE), percentage of landscape (PLAND), largest patch index (LPI), landscape shape index (LSI), patch density (PD), edge density (ED), area-weighted mean shape index (AWMSI), and patch cohesion index (COHESION) [34–36]. Collectively, these indices form the analytical framework for evaluating the spatial configuration of urban forest landscapes.

(1) CA represents the total area of all forest patches and is calculated as follows:

$$CA = \sum_{j=1}^{n} a_j \times 10,000 \quad (3)$$

where a_j is the area of the jth forest patch (in $\mathrm{m^2}$). The value is divided by 10,000 to convert the unit from square meters to hectares.

(2) TE denotes the total perimeter of all forest patches and is computed as follows:

$$TE = \sum_{j=1}^{n} p_j \tag{4}$$

where p_j is the perimeter of the jth forest patch.

(3) PLAND measures the proportion of the total landscape occupied by forest patches:

$$PLAND = \frac{\sum_{j=1}^{n} a_j}{A} \times 100 \tag{5}$$

where A is the total landscape area. The result is multiplied by 100 to express the value as a percentage.

(4) LPI quantifies the percentage of the landscape occupied by the largest forest patch:

$$LPI = \frac{max(a_1, \cdots, a_n)}{A} \times 100 \tag{6}$$

where $max\ (a_1, \cdots, a_n)$ is the area of the largest forest patch.

(5) LSI evaluates the complexity of patch shapes across the landscape:

$$LSI = \frac{0.25TE}{\sqrt{A}} \tag{7}$$

(6) PD reflects the number of forest patches per 100 hectares:

$$PD = \frac{n_i}{A} \times 10,000 \times 100 \tag{8}$$

where n_i is the number of forest patches. The result is scaled to units of number per 100 hectares.

(7) ED measures the total edge length of forest patches per hectare of landscape:

$$ED = \frac{\sum_{k=1}^{m} e_k}{A} \times 10,000 \tag{9}$$

where e_k is the edge length of the kth patch.

(8) AWMSI quantifies the average complexity of patch shapes, weighted by patch area:

$$AWMSI = \sum_{j=1}^{n} \left[\frac{0.25 p_j}{\sqrt{a_j}} \left(\frac{a_j}{\sum_{j=1}^{n} a_j} \right) \right] \tag{10}$$

(9) COHESION assesses the physical connectedness of forest patches:

$$COHESION = \left[1 - \frac{\sum_{j=1}^{n} p_{ij}}{\sum_{j=1}^{n} p_{ij} \times \sqrt{a_{ij}}} \right] \left[1 - \frac{1}{\sqrt{A}} \right]^{-1} \times 100 \tag{11}$$

The result is multiplied by 100 to express the index as a percentage, with higher values indicating greater connectivity and aggregation.

2.2.3. Pearson Correlation Analysis

In this study, a 1500 m × 1500 m fishnet grid was generated across the study area using ArcGIS 10.7. Grids containing incomplete or fragmented landscape boundaries were excluded, resulting in a total of 4667 valid sampling units. For each grid cell, the mean values of FVC and corresponding landscape metrics were extracted. Pearson correlation analysis was then employed to evaluate the relationships between forest landscape morphological characteristics and seasonal variations in FVC.

The Pearson correlation coefficient is fundamentally a linear correlation measure widely used in statistical analysis to quantify the linear relationship between interval variables [37,38]. For two given samples, $X = (x_1, x_2, \ldots, x_n)$ and $Y = (y_1, y_2, \ldots, y_n)$, the Pearson correlation coefficient is calculated as follows:

$$r = \frac{\sum_{i=1}^{n}(x_i - \overline{x})(y_i - \overline{y})}{\sqrt{\sum_{i=1}^{n}(x_i - \overline{x})^2 \sum_{i=1}^{n}(y_i - \overline{y})^2}} \quad (12)$$

In the formula, $\overline{x}$ and $\overline{y}$ represent the sample mean values of X and Y, respectively, while x_i and y_i denote the variable values of the two samples. The absolute value of the Pearson correlation coefficient r indicates the strength of the correlation between the independent and dependent variables. The range of values can be used to quantify the degree of correlation between the independent and dependent variables [39].

2.2.4. RF Regression Model

RF regression is an ensemble learning method based on decision trees that performs regression tasks by constructing a multitude of decision trees and aggregating their predictions to generate a final output [40,41]. Compared to traditional multiple linear regression, RF regression offers several notable advantages. First, it exhibits strong resistance to noise and robustness against data imperfections, such as missing values and outliers, which often compromise the performance of conventional regression models. Second, RF algorithms are capable of automatically identifying and ranking the importance of predictor variables, thereby facilitating the selection of key influencing factors. In contrast, traditional multiple regression typically relies on manual variable selection and is more vulnerable to multicollinearity among predictors. Furthermore, RF regression excels in handling high-dimensional datasets and effectively mitigates the risk of overfitting, a challenge commonly encountered in traditional regression models due to the "curse of dimensionality." Given these advantages, this study employs the RF regression model to quantitatively examine the relationship between landscape metrics and FVC. A corresponding modeling workflow was developed and illustrated to provide a systematic and reproducible framework for the analysis (Figure 3).

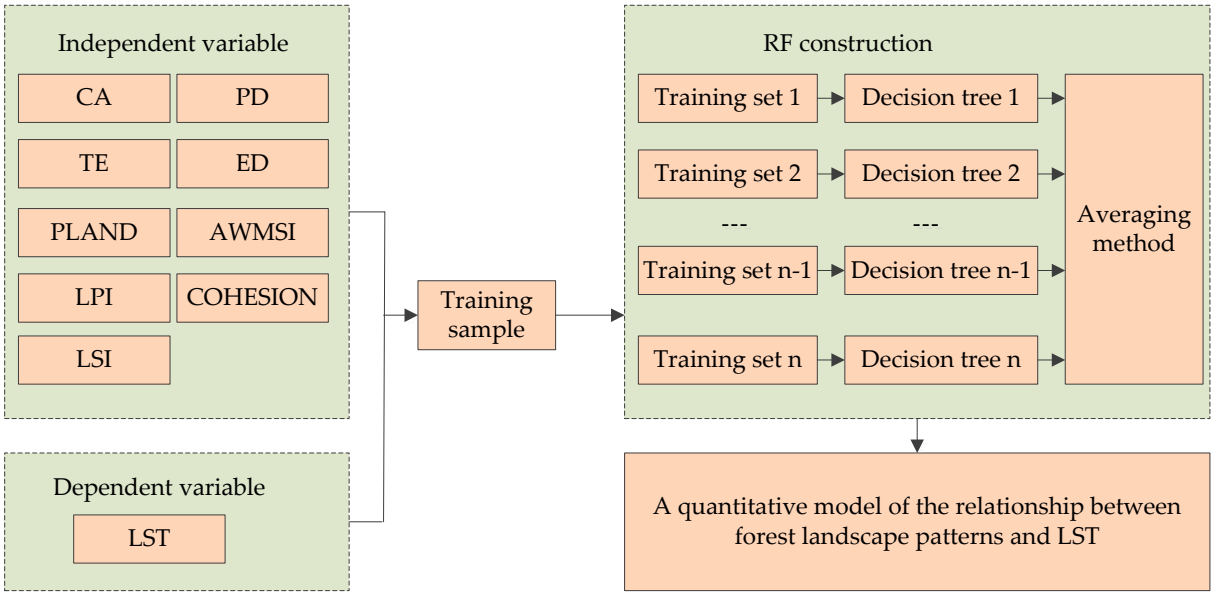

Figure 3. Process of RF regression model.

The Scientific Platform Serving for Statistics Professionals (SPSSPRO) is an online data analysis platform designed to offer convenient analytical services for statisticians, university faculty and students, market researchers, and scientific investigators [42]. In this study, the RF regression algorithm available on the SPSSPRO platform was employed to quantify the relative contribution of various landscape metrics to seasonal variations in FVC. The analysis was based on the seasonal mean values of FVC and corresponding landscape morphology indices within each grid cell.

The RF regression algorithm calculates feature importance in two primary steps: feature contribution assessment and importance normalization [43,44]. Initially, node splitting within each decision tree minimizes the mean square error (MSE) during model training. By aggregating the decrease in MSE for each feature across all decision trees, the contribution of individual features to the model is evaluated, a process referred to as mean decrease in impurity. Subsequently, the Permutation Importance method is employed, wherein the values of a feature are randomly shuffled, and the resulting change in the model's prediction error is observed. A larger increase in error indicates a greater influence of the feature on model predictions. Feature importance is then computed using these two methods and normalized to facilitate ranking, thereby identifying key variables and enhancing the interpretability of the model. In this study, feature importance was used to assess the contribution rate of the urban forest landscape morphology index to seasonal FVC.

The main parameters of the RF regression model were configured as follows: random shuffling of the data was enabled to enhance the model's generalization capability, and 70% of the total samples were allocated to the training set. Cross-validation was not employed. Node splitting was based on the MSE criterion, with all available features considered during each split. The minimum number of samples required to split an internal node was set to 2, while each leaf node contained at least 1 sample with no minimum sample weight constraint, ensuring a balance between model complexity and learning capacity. A total of 100 decision trees were constructed using bootstrap sampling with replacement; however, Out-of-Bag (OOB) error estimation was not activated. This parameter configuration was designed to achieve a trade-off between computational efficiency and model accuracy.

Model performance was evaluated using two widely adopted regression metrics: the MSE and Mean Absolute Error (MAE). The MSE emphasizes larger prediction errors by squaring them, making it more sensitive to outliers and useful for diagnosing overfitting to high-error samples. In contrast, the MAE measures the average absolute deviation between predicted and actual values, offering a more robust and interpretable assessment of overall prediction bias. These two indicators were used to quantitatively assess the predictive accuracy of the RF model on the test dataset, thereby enabling a comprehensive evaluation of its fitting performance and generalization ability. Notably, both metrics are inversely correlated with prediction accuracy—lower values indicate higher model performance.

3. Results

3.1. Spatiotemporal Distribution of FVC

The FVC was estimated using the pixel dichotomy model applied to Landsat imagery of Jinhua City. Seasonal FVC average values (Table 2) and distributions (Figure 4) for the year 2023 were subsequently derived. The results indicate that the highest average FVC was observed in summer (0.67), while the lowest occurred in winter (0.50). Among the four seasons, winter exhibited the greatest spatial variation in mean FVC across the study area, with an extreme difference of 0.36, whereas spring showed the smallest variation, with a difference of 0.18. At the administrative level, Pan'an County recorded the highest seasonal mean FVC in summer (0.80), while Jindong District registered the lowest in winter (0.35).

Table 2. Seasonal FVC average values of Jinhua in 2023.

City	Spring	Summer	Autumn	Winter
Jinhua	0.65	0.67	0.65	0.49
Wucheng	0.67	0.67	0.63	0.48
Jindong	0.58	0.57	0.56	0.35
Wuyi	0.73	0.74	0.69	0.50
Pujiang	0.74	0.73	0.71	0.58
Pan'an	0.67	0.80	0.79	0.71
Lanxi	0.63	0.62	0.60	0.43
Yiwu	0.56	0.55	0.54	0.35
Dongyang	0.64	0.66	0.67	0.54
Yongkang	0.58	0.61	0.59	0.43

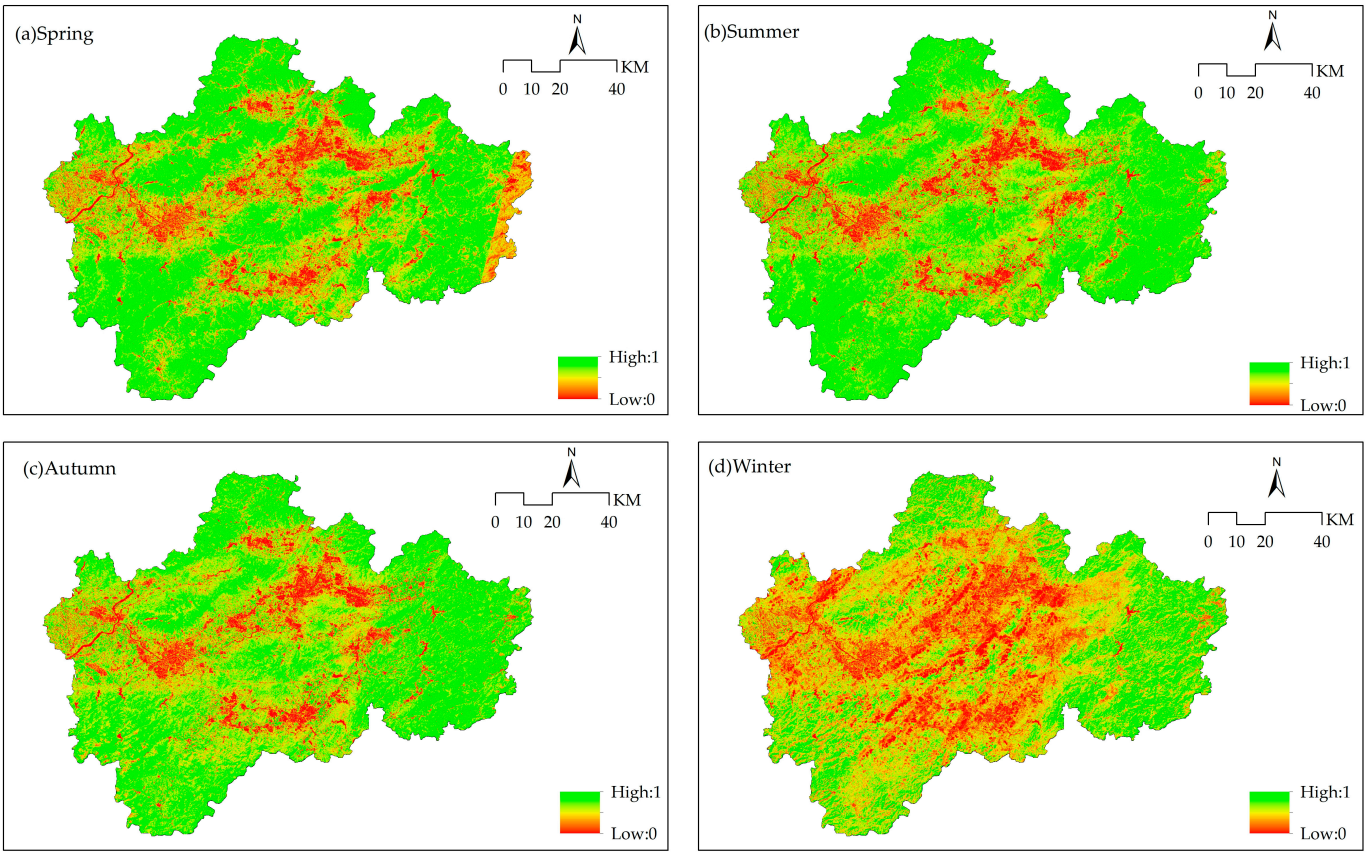

Figure 4. The seasonal FVC distribution maps of Jinhua in 2023.

3.2. Classification of FVC

To investigate the spatiotemporal dynamics of FVC, the calculated FVC values were categorized into distinct FVC levels (Figure 5). Subsequently, the areas corresponding to each FVC level were quantified, and their seasonal distributions were analyzed (Figure 6).

Seasonal variations in the areal distribution of FVC classes exhibited distinct spatial patterns. In spring, summer, and autumn, the rank order of FVC categories was very high coverage > high coverage > moderate coverage > very low coverage > low coverage. In contrast, during winter, the distribution shifted to:very low coverage > very high coverage > moderate coverage > low coverage > high coverage. The proportion of each FVC class varied markedly between seasons. In spring, areas classified as very high coverage accounted for the largest share (48.6%), followed by high coverage (20.6%), moderate coverage (12.5%), low coverage (7.7%), and very low coverage (10.6%). In summer, very

high coverage further increased to 50.6%, with the remaining classes comprising 25.2%, 10.5%, 5.2%, and 8.5%, respectively. In autumn, very high coverage declined slightly to 44.8%, while the other classes constituted 25.4%, 14.4%, 6.5%, and 9.0%. In winter, overall vegetation cover decreased substantially: very high coverage dropped to 22.3%, while very low coverage increased to 23.9%; the proportions of the remaining classes were 16.2%, 20.0%, and 17.7%, respectively.

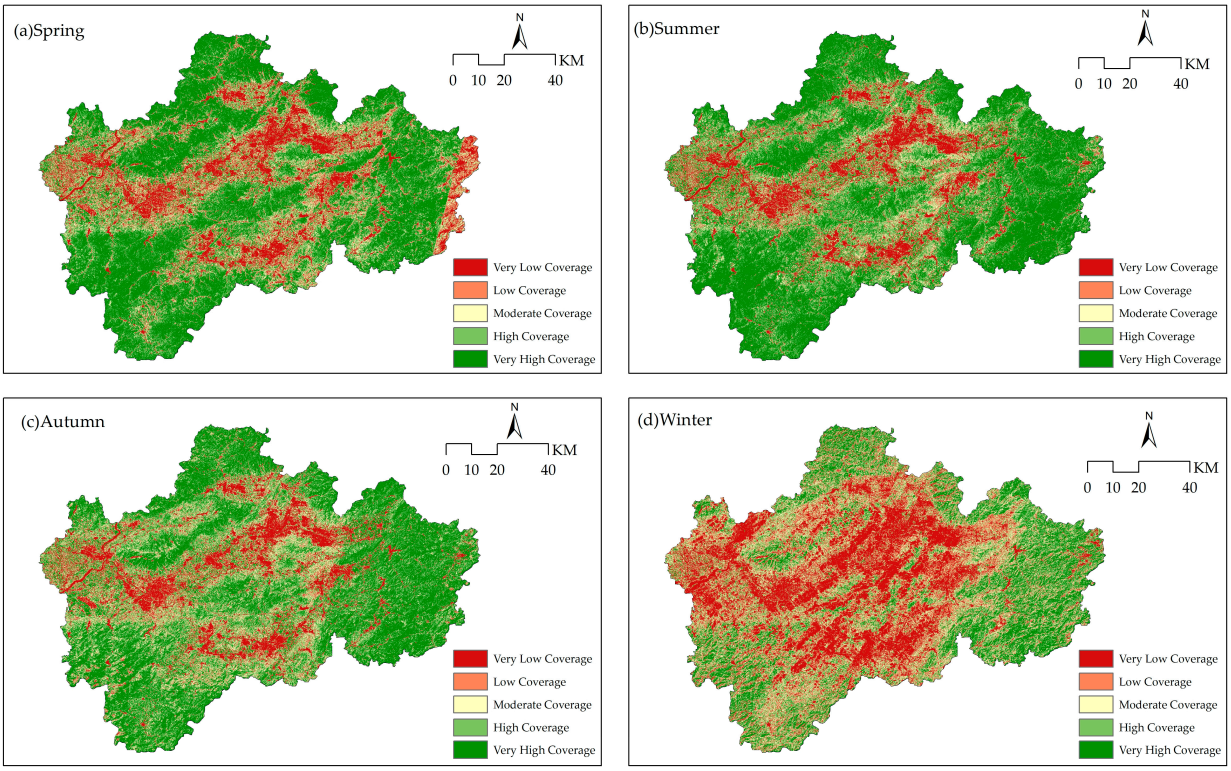

Figure 5. The seasonal FVC classification of Jinhua in 2023.

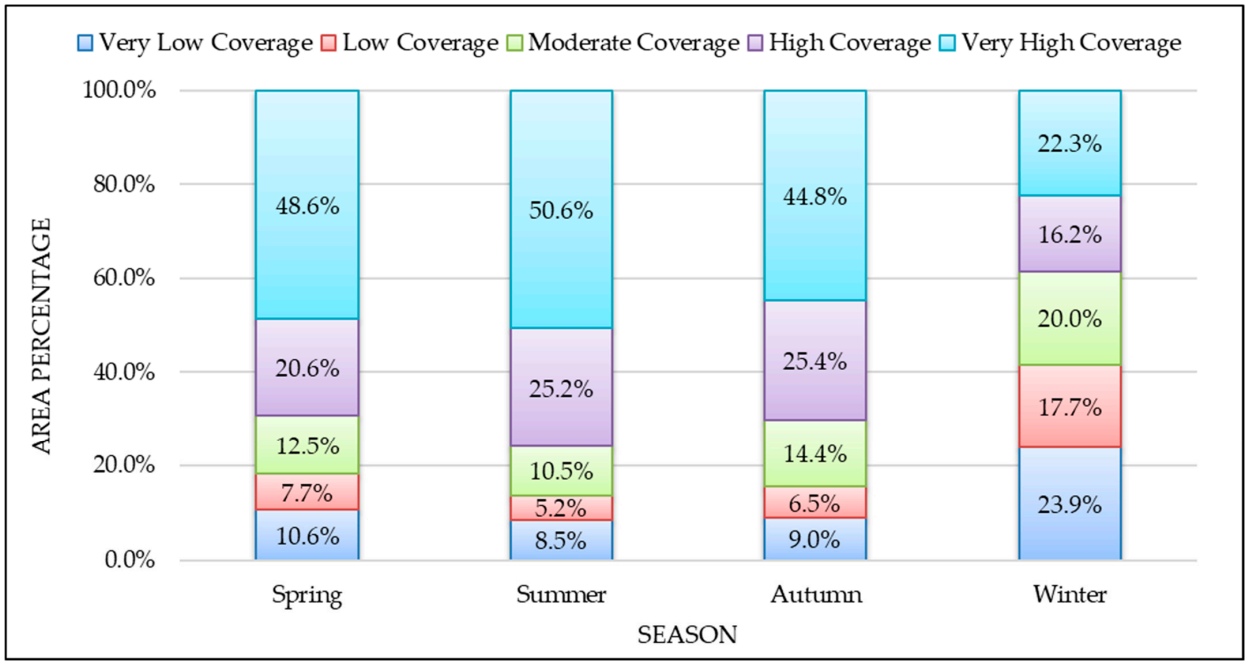

Figure 6. The proportion of area covered by different FVC levels across seasons in 2023.

The seasonal average FVC across different land use types (Table 3) followed the order forest > cropland > water > impervious surfaces. Among these, forests exhibited the highest average FVC in summer, reaching 0.79, whereas water recorded the lowest average FVC in winter, at only 0.01. From a seasonal perspective, the FVC of forested areas displayed clear temporal variation, with values ranked in the order of summer > spring > autumn > winter, indicating pronounced seasonal dynamics in vegetation cover.

Table 3. Seasonal average FVC of different land use types.

Land Use Type	Spring	Summer	Autumn	Winter
Cropland	0.53	0.60	0.59	0.37
Forest	0.77	0.79	0.76	0.63
Water	0.04	0.05	0.02	0.01
Impervious surfaces	0.14	0.15	0.13	0.12

3.3. Pearson Correlation Analysis of Seasonal FVC and Landscape Metrics

The spatial distribution of nine landscape metrics in the study area was derived using Fragstats 4.2 software (Figure 7). The indices—CA, PLAND, LPI, and COHESION—exhibited relatively high values across most regions, indicating their strong capacity to characterize the forest landscape pattern. In contrast, the spatial distributions of PD, TE, LSI, ED, and AWMSI were more uniform, reflecting higher spatial homogeneity across the study area.

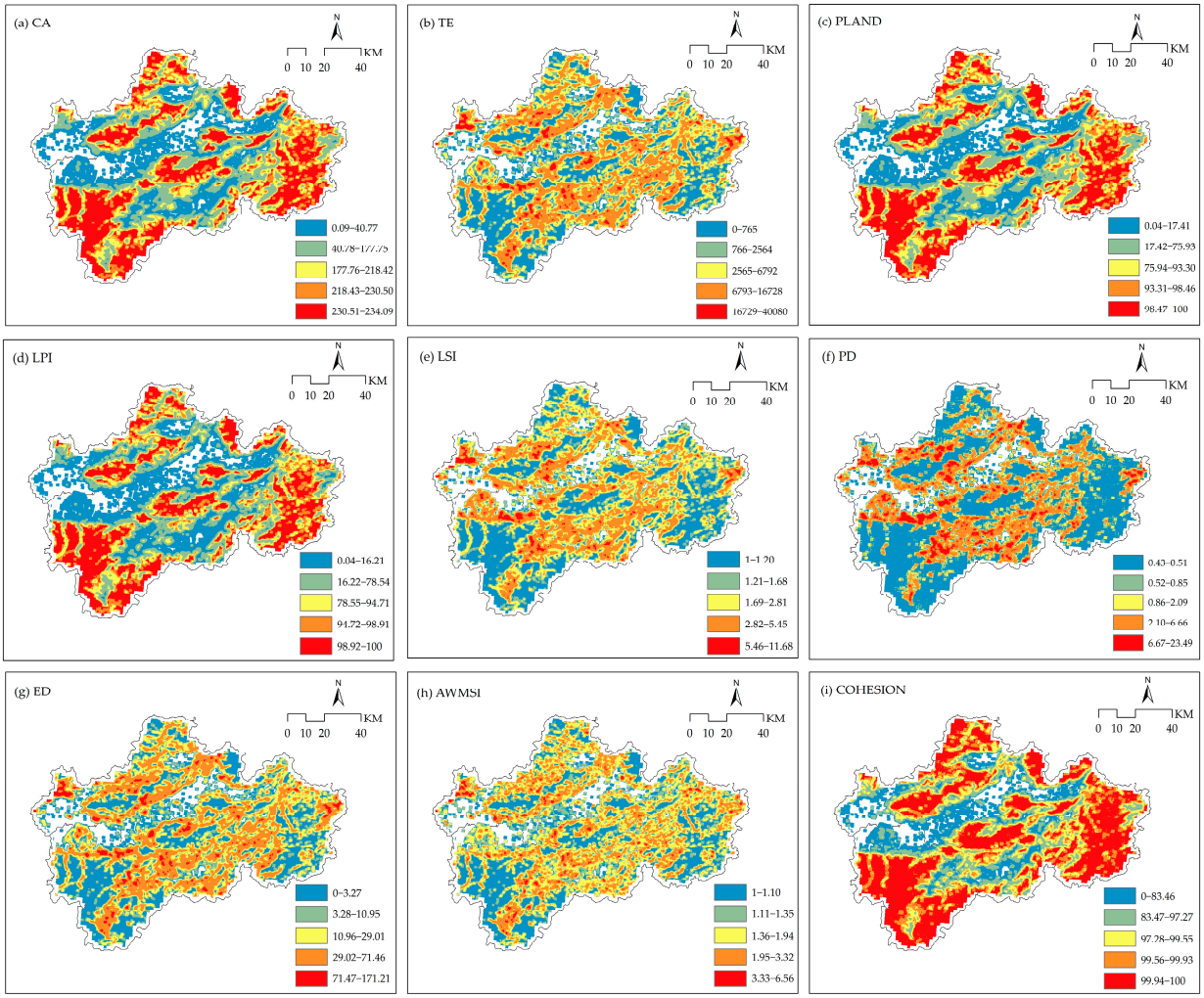

Figure 7. Spatial distribution of landscape metrics in 2023.

Pearson correlation analysis was conducted to explore the relationship between seasonal FVC and landscape metrics (Table 4). The results indicate that all landscape morphology indices are significantly correlated with seasonal FVC ($p < 0.01$). Specifically, CA, PLAND, LPI, and COHESION demonstrated significant positive correlations with FVC, suggesting that larger forest core areas, higher landscape proportions, stronger patch dominance, and greater connectivity contribute to increased vegetation cover. Conversely, TE, LSI, PD, ED, and AWMSI showed significant negative correlations with FVC, implying that more fragmented and complex landscape configurations are associated with reduced FVC.

Table 4. Seasonal FVC and forest landscape indices Pearson correlation coefficients.

Landscape Indices	Spring	Summer	Autumn	Winter
CA	0.842	0.826	0.799	0.731
TE	−0.113	−0.092	−0.072	−0.120
PLAND	0.842	0.826	0.799	0.731
LPI	0.838	0.820	0.793	0.730
LSI	−0.352	−0.321	−0.305	−0.346
PD	−0.354	−0.324	−0.324	−0.368
ED	−0.113	−0.092	−0.072	−0.120
AWMSI	−0.088	−0.070	−0.041	−0.072
COHESION	0.656	0.662	0.643	0.558

The strength of correlations between the landscape metrics and FVC varied seasonally. CA, PLAND, and LPI exhibited very strong correlations with FVC during spring and summer, while maintaining strong correlations in autumn and winter. COHESION displayed a strong correlation with FVC in spring, summer, and fall, but weakened to a moderate level in winter. In contrast, the LSI and PD consistently showed weak correlations with FVC across all seasons. TE, ED, and AWMSI exhibited very weak correlations with FVC throughout the year, suggesting that these indices contribute minimally to seasonal variations in vegetation cover.

3.4. Contribution Rate of Landscape Metrics to Seasonal FVC

To evaluate the predictive performance of the RF regression model across different seasons, two key metrics—MSE and MAE—were employed for quantitative analysis (Table 5). The results indicate that the model achieved its highest performance during the summer, exhibiting the lowest MSE and MAE values among all seasons, thereby reflecting the smallest prediction error and the highest model reliability. Overall, the RF regression model maintained consistently low prediction errors throughout the year, demonstrating its strong predictive accuracy and robustness across seasonal variations.

Table 5. Evaluation of the predictive effect of RF regression model.

Season	Dataset	MSE	MAE
Spring	Test set	0.010	0.071
Summer	Test set	0.009	0.070
Autumn	Test set	0.011	0.082
Winter	Test set	0.017	0.105

The RF regression model was applied to analyze the contributions of landscape metrics to seasonal FVC in Jinhua City (Figure 8).

In spring, the PLAND for forests reached 45.4%, indicating a widespread distribution across the region. However, the CA accounted for only 34.3%, suggesting that despite high

overall coverage, forests were predominantly distributed as small or scattered patches, lacking large contiguous areas.

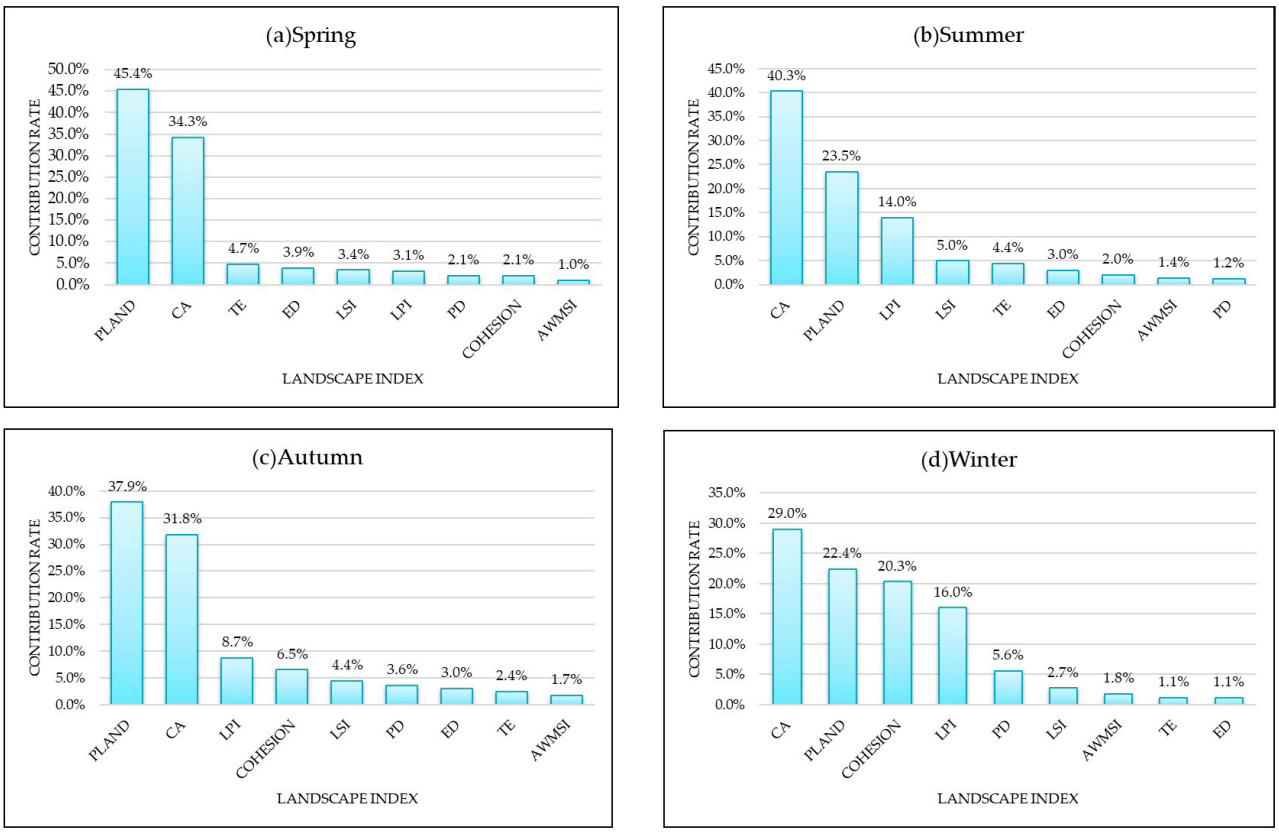

Figure 8. The contribution rate of the forest landscape morphology index to FVC.

During summer, the CA of forests increased substantially to 40.3%, surpassing the PLAND value of 23.5%. This shift reflects not only a broader spatial extent but also a more concentrated patch distribution. The LPI rose to 14.0%, signifying the presence of large core forest patches that substantially contributed to overall vegetation cover. This concentration of large patches enhanced spatial cohesion. Meanwhile, the LSI accounted for 5.0%, indicating moderate morphological complexity with low fragmentation.

In autumn, forest PLAND and CA were measured at 37.9% and 31.8%, respectively, demonstrating that forest cover remained substantial and relatively concentrated, though some patch fragmentation persisted. The LPI represented 8.7%, highlighting the dominance of large forest patches, while COHESION reached 6.5%, suggesting good spatial connectivity and a relatively intact ecological function among forest patches.

In winter, the CA declined to 29.0%, and PLAND decreased to 22.4%, reflecting a reduction in forest cover, primarily concentrated in contiguous patches with fewer scattered fragments. Notably, COHESION increased to 20.3%, signifying enhanced spatial connectivity and improved ecological coherence of forest patches. The LPI also increased to 16.0%, indicating that large forest patches remained dominant. PD accounted for just 5.6%, suggesting lower fragmentation during the winter months.

A comprehensive analysis across all seasons indicates varying contributions of the nine landscape metrics to FVC. Among these, CA and PLAND demonstrated the most significant contributions to FVC, followed by COHESION and LPI. In contrast, PD, AWMSI, LSI, TE, and ED showed relatively low contributions. It is noteworthy that synergistic interactions may exist among these landscape indices, potentially influencing their collective impact on FVC. Further investigation is required to elucidate these combined effects.

4. Discussion

This study investigates the spatial and temporal dynamics of FVC across four seasons—spring, summer, autumn, and winter—in Jinhua City during 2023. The results indicate that the seasonal average FVC follows the order summer > spring > autumn > winter. In terms of spatial distribution, areas with very high and high vegetation coverage collectively accounted for over 69% of the total area during spring, summer, and autumn, while this proportion dropped significantly to 38.5% in winter, highlighting a marked seasonal variability. Pearson correlation analysis revealed that forest landscape indices including CA, PLAND, LPI, and COHESION exhibited significant positive correlations with FVC across all seasons. This suggests that increases in the patch size, area share, maximum patch dominance, and spatial connectivity of forested areas contribute positively to vegetation cover. Conversely, TE, LSI, PD, ED, and AWMSI were significantly negatively correlated with FVC, implying that greater landscape complexity and fragmentation tend to suppress vegetation cover.

To further explore the relative importance of these landscape metrics, a RF regression model was employed. The results showed that the contribution of landscape indices to seasonal FVC varied, with CA and PLAND consistently ranking as the top two contributors. These findings are in line with the correlation analysis and can be attributed to the fact that forests, as high-coverage vegetation types, contribute extensively to regional greenness. Larger CA values indicate broader vegetation-covered areas, enhancing ecological connectivity and landscape-level greenness [45,46]. Similarly, higher PLAND values suggest a more continuous and aggregated forest landscape, which reduces land surface exposure and fragmentation, thereby supporting ecosystem stability and vegetation growth [47,48]. COHESION and LPI ranked third and fourth in importance, respectively. COHESION reflects the degree of spatial connectivity among forest patches, which is crucial for maintaining ecological processes and system resilience, thereby promoting sustained vegetation growth [49]. The LPI represents the area proportion of the largest forest patch, and larger contiguous patches typically provide more stable habitats and favorable hydrothermal conditions conducive to higher vegetation cover [50]. In contrast, the contributions of PD, AWMSI, LSI, TE, and ED were relatively lower. Although these indices are valuable in describing landscape configuration and edge complexity, their direct influence on vegetation cover appears to be more limited in this context.

The main findings of this study provide valuable scientific insights for urban forest planning and management. Previous research has demonstrated that expanding urban forest areas is an effective strategy for increasing urban FVC [51]. Generally, higher proportions of urban forest coverage are associated with greater FVC [52,53]. However, due to constraints on urban land and high construction density, expanding forested areas is increasingly challenging [54]. Thus, optimizing the spatial layout of existing forests emerges as a more practical and efficient solution. Pearson correlation and RF regression analyses suggest that prioritizing large, compact, and highly aggregated forest patches can significantly enhance urban FVC.

Although this study has produced meaningful findings, certain limitations remain. Future research should focus on two key improvements: (1) Incorporating the fishing net division method to construct irregular grid cells for evaluating the impact of different grid configurations on seasonal FVC dynamics. (2) Investigating the nonlinear relationship between landscape metrics and seasonal FVC, with a particular emphasis on identifying potential influence thresholds. These advancements are expected to improve the scientific basis for urban forest planning and provide more precise decision-making support for optimizing FVC.

5. Conclusions

This study, grounded in multi-source remote sensing data and landscape ecology theory, focuses on Jinhua City to analyze seasonal variations in FVC. Using the GEE platform, FVC was calculated and classified into different coverage levels. A forest landscape morphology index system was constructed based on nine representative indices. Pearson correlation analysis was employed to examine the relationships between seasonal FVC and landscape metrics, while the RF regression model was applied to quantify the contributions of each index to seasonal FVC.

This study revealed that in Jinhua, areas classified as very high coverage and high coverage collectively accounted for more than 69% of the total area during spring, summer, and autumn, whereas this proportion declined sharply to 38.5% in winter. All landscape metrics exhibited significant correlations with seasonal FVC. Specifically, CA, PLAND, LPI, and COHESION were significantly and positively correlated with FVC, indicating that larger and more cohesive forest patches contribute to higher FVC. Conversely, TE, LSI, PD, ED, and AWMSI were significantly and negatively correlated with FVC, reflecting that more fragmented and irregular forest landscapes tend to inhibit FVC. Nine landscape metrics contributed differently to FVC. Among them, CA and PLAND were the most influential, followed by COHESION and LPI. In contrast, PD, AWMSI, LSI, TE, and ED exhibited relatively low contributions to FVC.

This study provides a scientific basis for understanding the influence mechanisms of landscape metrics on seasonal FVC in Jinhua City. It also offers valuable insights for optimizing landscape indices and managing FVC in similar urban environments. Moreover, the integration of multi-source remote sensing data with landscape metrics demonstrates strong generalizability and applicability for assessing FVC in different urban contexts.

Author Contributions: Data curation, Y.Z.; investigation, S.C.; methodology, H.Y.; project administration, H.Y.; resources, H.Z.; software, H.Z.; visualization, Y.Z.; writing—original draft, H.Y.; writing—review and editing, S.C.; H.Y. is responsible for future questions from readers as the corresponding author. All authors have read and agreed to the published version of the manuscript.

Funding: This research is funded by Communication University of Zhejiang Horizontal Major Research Project (grant number Z421A23017); Zhejiang Provincial Natural Science Foundation of China (grant number LTGG24F030002); 2024 Communication University of Zhejiang Young Faculty Research Enhancement Program Project (grant number Z431Q25010G); the Zhejiang Key Laboratory of Film and TV Media Technology (2024E10023); and Intelligent Media Engineering Research Center of Zhejiang Province.

Data Availability Statement: The data are not publicly available due to privacy. The data presented in this paper are available on request from the corresponding author.

Conflicts of Interest: The authors declare no conflicts of interest.

References

1. Wang, M.; Liu, J. Evaluation of the potential effects of forest vegetation cover on surface temperature in different geographical and climatic regions of Shaanxi Province, China. *CATENA* **2025**, *255*, 109020.
2. Chen, L.; Li, C.; Pan, C.; Yan, Y.; Jiao, J.; Zhou, Y.; Wang, X.; Zhou, G. Estimating the Effects of Natural and Anthropogenic Activities on Vegetation Cover: Analysis of Zhejiang Province, China, from 2000 to 2022. *Remote Sens.* **2025**, *17*, 1433.
3. Yao, Y.; Yan, J.; Li, G.; Ma, W.; Yao, X.; Song, M.; Li, Q.; Li, J. A GNSS-IR Soil Moisture Inversion Method Considering Multi-Factor Influences Under Different Vegetation Covers. *Agriculture* **2025**, *15*, 837.
4. Gu, R.; Li, X.; Liu, B.; Li, H.; Zhang, Z.; Liu, Y. The crucial role of vegetation cover in shaping the dipole pattern of East Asian summer monsoon changes during the late Pliocene warm period. *Quat. Sci. Rev.* **2025**, *357*, 109317.
5. Hickman, I.; Camac, J.; Venn, S.; Morgan, J. Long-term alpine summit vegetation cover change: Divergent trajectories driven by climate warming and fire. *Arct. Antarct. Alp. Res.* **2025**, *56*, 2429864.

6. Sofue, Y.; Kohsaka, R. Vegetation cover survey methods at cross-roads: Choice of aerial photography or satellite imagery by Japanese municipalities. *Environ. Sustain. Indic.* **2024**, *24*, 100471.
7. Yang, R.; Li, S.; Zhang, B.; Jiao, Q.; Peng, D.; Yang, S.; Yu, R. A Multispectral Feature Selection Method Based on a Dual-Attention Network for the Accurate Estimation of Fractional Vegetation Cover in Winter Wheat. *Remote Sens.* **2024**, *16*, 4441.
8. Roman, L.A.; Catton, I.J.; Greenfield, E.J.; Pearsall, H.; Eisenman, T.S.; Henning, J.G. Linking Urban Tree Cover Change and Local History in a Post-Industrial City. *Land* **2021**, *10*, 403. [CrossRef]
9. Zhao, Y.; Xu, S.; Huang, Z.; Fang, W.; Huang, S.; Huang, P.; Zheng, D.; Dong, J.; Chen, Z.; Yan, C.; et al. Temporal and Spatial Characteristics of Soundscape Ecology in Urban Forest Areas and Its Landscape Spatial Influencing Factors. *Forests* **2022**, *13*, 1751. [CrossRef]
10. Osewe, E.; Popa, B.; Kagombe, J.; Osewe, I.; Abrudan, I. Ecosystem services values for local people in participatory forestry context: The case of karura urban forest reserve. *Trees For. People* **2025**, *20*, 100834.
11. Morato, K.; Morante, J.; Cabral, J.; Heming, N.; Faria, D. Landscape forest cover and local vegetation structure mediate multitrophic relationships but not the leaf damage in cacao trees. *For. Ecol. Manag.* **2024**, *572*, 122286.
12. Lin, Y.; Jin, Y.; Ge, Y.; Hu, X.; Weng, A.; Wen, L.; Zhou, Y.; Li, B. Insights into forest vegetation changes and landscape fragmentation in Southeastern China: From a perspective of spatial coupling and machine learning. *Ecol. Indic.* **2024**, *166*, 112479.
13. Joshi, A.; Ratnam, J.; Paramjyothi, H.; Sankaran, M. Climate and vegetation collectively drive soil respiration in montane forest-grassland landscapes of the southern Western Ghats, India. *J. Trop. Ecol.* **2024**, *40*, e16.
14. Li, Y.; Xue, C.; Shao, H.; Shi, G.; Jiang, N. Study of the Spatiotemporal Variation Characteristics of Forest Landscape Patterns in Shanghai from 2004 to 2014 Based on Multisource Remote Sensing Data. *Sustainability* **2018**, *10*, 4397. [CrossRef]
15. Wang, H.; Wang, H.; Chen, S.; Luo, X.; Liu, B.; Tian, X.; Feng, Y.; Wang, P. Dynamic Change Analysis of Vegetation Coverage and Landscape Pattern Characteristics in Longquan Mountain Urban Forest Park, Chengdu City. *Remote Sens. Technol. Appl.* **2023**, *38*, 1455–1466.
16. Duo, L.; Li, Y.; Zhang, M.; Zhao, Y.; Wu, Z.; Zhao, D. Spatiotemporal Pattern Evolution of Urban Ecosystem Resilience Based on "Resistance-Adaptation-Vitality": A Case Study of Nanchang City. *Front. Earth Sci.* **2022**, *10*, 902444.
17. Byrne, G.; Broomhall, M.; Walsh, A.J.; Thankappan, M.; Hay, E.; Li, F.; McAtee, B.; Garcia, R.; Anstee, J.; Kerrisk, G.; et al. Validating Digital Earth Australia NBART for the Landsat 9 Underfly of Landsat 8. *Remote Sens.* **2024**, *16*, 1233.
18. Zhao, F.; Xia, L.; Kylling, A.; Li, R.; Shang, H.; Xu, M. Detection flying aircraft from Landsat 8 OLI data. *ISPRS J. Photogramm. Remote Sens.* **2018**, *141*, 176–184.
19. Stuart, W.; Hossain, A.K.M.A.; Hunt, N.; Mix, C.; Qin, H. Spatiotemporal Analysis of Urban Forest in Chattanooga, Tennessee from 1984 to 2021 Using Landsat Satellite Imagery. *Remote Sens.* **2024**, *16*, 2419.
20. Jinhua Overview. Available online: https://www.jinhua.gov.cn/col/col1229159908/index.html (accessed on 20 February 2025).
21. Yang, H.; Zeng, H.; Chu, S.; Zhao, Y.; Cai, X. Analysis of Morphological Impacts on Cooling Effects of Urban Water Bodies in Five Cities of Zhejiang. *Water* **2025**, *17*, 80.
22. 2013 Jinhua Municipal National Economic and Social Development Statistical Bulletin. Available online: http://tjj.jinhua.gov.cn/art/2014/2/12/art_1229317894_2979239.html (accessed on 12 February 2014).
23. 2023 Jinhua Municipal National Economic and Social Development Statistical Bulletin. Available online: http://tjj.jinhua.gov.cn/art/2024/5/9/art_1229317894_4154037.html (accessed on 9 May 2024).
24. Gu, H.; Zhang, W. Quantitative assessment of urban-rural spatiotemporal heterogeneity in air pollutants using GEE multi-source data across the Anhui province, China. *Atmos. Pollut. Res.* **2025**, *16*, 102464.
25. The 30 m Annual Land Cover Datasets and Its Dynamics in China from 1985 to 2023. Available online: https://zenodo.org/records/12779975 (accessed on 1 August 2024).
26. Zang, Y.; Wang, K.; Xu, S.; Xiao, W.; Tong, T.; Sun, H.; Li, C. Identification of surface mining and assessment of ecological restoration effects using GEE and Sentinel-2 image data—A case study on Yangtze River watershed, China. *Ecol. Eng.* **2025**, *212*, 107525.
27. Singh, B.M.; Komal, C.; Victorovich, K.A. Crop growth monitoring through Sentinel and Landsat data based NDVI time-series. *Comput. Opt.* **2020**, *44*, 409–419.
28. Hernández-López, D.; Piedelobo, L.; Moreno, M.A.; Chakhar, A.; Ortega-Terol, D.; González-Aguilera, D. Design of a Local Nested Grid for the Optimal Combined Use of Landsat 8 and Sentinel 2 Data. *Remote Sens.* **2021**, *13*, 1546.
29. Huang, S.; Tang, L.; Hupy, J.; Wang, Y.; Shao, G. A commentary review on the use of normalized difference vegetation index (NDVI) in the era of popular remote sensing. *J. For. Res.* **2021**, *32*, 1–6.
30. Zea, P.; Pascual, C.; García-Montero, L.G.; Cedillo, H. NDVI Performance for Monitoring Agricultural Energy Inputs Using Landsat Imagery: A Study in the Ecuadorian Andes (2012–2023). *Sustainability* **2025**, *17*, 3480. [CrossRef]
31. Yao, Y.; Shen, J.; Yue, J.; Liu, Y.; Feng, H.; Shu, M.; Fu, Y.; Qiao, H.; Sun, T.; Zheng, G. Remotely estimate the cropland fractional vegetation cover using linear spectral mixture analysis and improved band operations. *Int. J. Remote Sens.* **2025**, *46*, 3466–3486.

32. Liu, Z.; Bi, H.; Zhao, D.; Guan, N.; Wang, N.; Song, Y. Determination of Fractional Vegetation Cover Threshold Based on the Integrated Synergy–Supply Capacity of Ecosystem Services. *Forests* **2025**, *16*, 587. [CrossRef]
33. Lin, R.; Xu, X.; Zhang, X.; Hu, Z.; Wang, G.; Shi, Y.; Zhao, X.; Sang, H. Surface Soil Moisture Estimation Taking into Account the Land Use and Fractional Vegetation Cover by Multi-Source Remote Sensing. *Agriculture* **2025**, *15*, 497. [CrossRef]
34. He, Z.; Lin, Z.; Xu, Q.; Ding, S.; Bao, X.; Li, X.; Hu, X.; Li, J. Multi-Dimensional Landscape Connectivity Index for Prioritizing Forest Cover Change Scenarios: A Case Study of Southeast China. *Forests* **2024**, *15*, 1490. [CrossRef]
35. Zhong, J.; Li, X.; Liu, W.; Zhang, F.; Huang, F.; Xu, S.; Xiao, S.; Wang, Q. Effects of urbanization intensity on forest vegetation characteristics and landscape pattern indices in Nanchang. *Chin. J. Ecol.* **2024**, *43*, 2285–2294.
36. Malcangi, F.; Lindén, A.; Sundell, J.; Loehr, J. Correlation between mammal track abundance and Forest Landscape Integrity Index validates actual forest ecological integrity. *Oecologia* **2024**, *206*, 61–72.
37. He, X.; Huang, B.; Peng, L.; Chen, J. Studies on Submersible Short-Circuit Blowing Based on Orthogonal Experiments, Back Propagation Neural Network Prediction, and Pearson Correlation Analysis. *Appl. Sci.* **2024**, *14*, 10321.
38. Wang, X.; Yao, Y.; Li, Z.; Su, C.; Tian, Y. Protocol Reverse Analysis of Ethernet for Control Automation Technology Based on Sequence Alignment and Pearson Correlation Coefficient. *Sensors* **2024**, *24*, 7922. [CrossRef]
39. Shi, Z.; Xiao, J.; Jiang, J.; Zhang, Y.; Zhou, Y. Identifying Reliability High-Correlated Gates of Logic Circuits with Pearson Correlation Coefficient. *IEEE Trans. Circuits Syst. II* **2024**, *71*, 2319–2323.
40. Zhao, Z.; Kantono, K.; Kam, R.; Le, T.T.; Kitundu, E.; Chen, T.; Hamid, N. Improving the Bioactivities of Apricot Kernels Through Fermentation: Investigating the Relationship Between Bioactivities, Polyphenols, and Amino Acids Through the Random Forest Regression XAI Approach. *Foods* **2025**, *14*, 845. [CrossRef]
41. Qiao, Y.; Sun, H.; Qi, J.; Liu, S.; Li, J.; Ji, Y.; Wang, H.; Peng, Y. Examining water bodies' cooling effect in urban parks with buffer analysis and random forest regression. *Urban Clim.* **2025**, *59*, 102301.
42. Fan, C.; Wu, Q.; Zhang, G.; Zeng, J. Construction and test of mango fruit shape identification platform based on 3D point cloud data. *Trans. Chin. Soc. Agric. Eng.* **2024**, *40*, 290–296.
43. Zhang, Y.; Ge, J.; Bai, X.; Wang, S. Blue-Green space seasonal influence on land surface temperatures across different urban functional zones: Integrating Random Forest and geographically weighted regression. *J. Environ. Manag.* **2025**, *374*, 123975.
44. Brown, M.; Peterson, M.; Tezaur, I.; Peterson, K.; Bull, D. Random forest regression feature importance for climate impact pathway detection. *J. Comput. Appl. Math.* **2025**, *464*, 116479.
45. Scriven, S.; Carlson, K.; Hodgson, J.; McClean, C.; Heilmayr, R.; Lucey, J.; Hill, J. Testing the benefits of conservation set-asides for improved habitat connectivity in tropical agricultural landscapes. *J. Appl. Ecol.* **2019**, *56*, 2274–2285. [PubMed]
46. Cui, L.; Zhao, Y.; Liu, J.; Wang, H.; Han, L.; Li, J.; Sun, Z. Vegetation Coverage Prediction for the Qinling Mountains Using the CA–Markov Model. *ISPRS Int. J. Geo-Inf.* **2021**, *10*, 679.
47. Yirigui, Y.; Lee, S.-W.; Nejadhashemi, A.P. Multi-Scale Assessment of Relationships between Fragmentation of Riparian Forests and Biological Conditions in Streams. *Sustainability* **2019**, *11*, 5060. [CrossRef]
48. Zhao, J.; Liu, S.; Wang, Z.; Gao, H.; Feng, S.; Wei, B.; Hou, Z.; Xiao, F.; Jing, L.; Liao, X. The Impact of Land Use and Landscape Pattern on Ecosystem Services in the Dongting Lake Region, China. *Remote Sens.* **2023**, *15*, 2228.
49. Calamari, N.; Vilella, F.; Sica, Y.; Mercuri, P. Patch and landscape responses of bird abundance to fragmentation in agroecosystems of east-central Argentina. *Avian Conserv. Ecol.* **2019**, *13*, 3.
50. Faye, B.; Du, G.; Li, Q.; Faye, H.V.M.T.; Diéne, J.C.; Mbaye, E.; Seck, H.M. Lessons Learnt from the Influencing Factors of Forested Areas' Vulnerability under Climatic Change and Human Pressure in Arid Areas: A Case Study of the Thiès Region, Senegal. *Appl. Sci.* **2024**, *14*, 2427.
51. Wang, F.; Wang, K. Assessing the Effect of Eco-City Practices on Urban Sustainability Using an Extended Ecological Footprint Model: A Case Study in Xi'an, China. *Sustainability* **2017**, *9*, 1591.
52. Lee, P.S.-H.; Park, J. An Effect of Urban Forest on Urban Thermal Environment in Seoul, South Korea, Based on Landsat Imagery Analysis. *Forests* **2020**, *11*, 630. [CrossRef]
53. Cao, W.; Huang, L.; Liu, L.; Zhai, J.; Wu, D. Overestimating Impacts of Urbanization on Regional Temperatures in Developing Megacity: Beijing as an Example. *Adv. Meteorol.* **2019**, *2019*, 3985715.
54. Jaworek-Jakubska, J.; Filipiak, M.; Michalski, A.; Napierała-Filipiak, A. Spatio-Temporal Changes of Urban Forests and Planning Evolution in a Highly Dynamical Urban Area: The Case Study of Wrocław, Poland. *Forests* **2020**, *11*, 17.